An experimental database for benchmarking simulations of turbulent premixed reacting flows: lean extinction limits and velocity field measurements in a dump combustor

P.D. Nguyen, Pascal Bruel, S. Reichstadt

An Experimental Database for Benchmarking Simulations of Turbulent Premixed Reacting Flows: Lean Extinction Limits and Velocity Field Measurements in a Dump Combustor

NGUYEN, P.D.[1,2] - BRUEL, P.[1] and REICHSTADT, S.[1]

[1] Laboratoire de Mathématiques et de leurs Applications

UMR 5142 CNRS-UPPA

Université de Pau et des Pays de l'Adour

IPRA, BP 1155, 64000 Pau Cedex – France

Corresponding author:

BRUEL, P.

Laboratoire de Mathématiques et de leurs Applications de Pau

CNRS - Université de Pau et des Pays de l'Adour (UMR 5142)

IPRA, BP 1155, 64000 Pau Cedex – France

Tel.: (+33) (0) 5 5940 7552, Fax: (+33) (0) 5 5940 7555

E-mail: Pascal.Bruel@univ-pau.fr

[2] On leave from the Department of Mechanical Engineering, Ho Chi Minh City University of Industry, Viet Nam.

Abstract

This contribution is aimed at drawing the attention of the CFD community on the availability of an experimental database regarding turbulent lean premixed prevaporised (LPP) reacting flows stabilised behind a double symmetric, plane sudden expansion fed by two fully developed turbulent channel flows of air plus propane. This flow configuration can be thought of as a relevant benchmark for testing turbulence and/or combustion models aimed at helping for the design of reliable LPP combustion chambers. This database contains a large amount of raw and processed data regarding essentially the velocity field for one inert and three different reacting flows configurations. Additional pieces of information are available and concern the lean extinction properties and the wall static pressure evolution in the feeding channels. For the reacting flows, the presence of a large scale coherent motion is clearly visible in the velocity spectra and it is shown how a data processing based on the semi-deterministic approach (SDA) that decomposes the velocity signal into the sum of its steady time average, its coherent fluctuations and its stochastic fluctuations can permit to evaluate their respective contribution to the total velocity fluctuations.

Key words: coherent motion, LDV, lean extinction, LPP combustor, premixed combustion, semi-deterministic approach.

Nomenclature

$A_r=1+2h/(2H+h_p)=1.84$		Expansion ratio
$h=0.0299$	[m]	Step height
$h_p=0.01$	[m]	Splitter plate thickness
$H=0.0304$	[m]	Height of each inlet channel
Q	[kg/s]	Mass flow rate
x	[m]	Streamwise coordinate (The dump plane is at x=0m)
y	[m]	Normal coordinate
$y^* = (y-y^{wall}_{lo})/(y^{wall}_{up}-y^{wall}_{lo})$		Reduced normal coordinate relative to each inlet channel
y^{wall}_{up}, y^{wall}_{lo}	[m]	Upper and lower wall normal coordinates.
u, v	[m/s]	Streamwise and normal velocity components
$W = 0.1505$	[m]	Inlet channel cross-section width
$\nu_0 = 13.75\ 10^{-6}$	[m^2/s]	Kinematic viscosity coefficient of the incoming streams
$Re = U_{bulk}H/\nu_0$	[-]	Bulk Reynolds number for each inlet stream
Φ	[-]	Equivalence ratio based on the global formula of the fuel

Subscripts:

$_L$	Relative to the lower stream
$_{lo}$	Relative to the lower wall of an inlet channel
$_p$	Relative to periodic motion
$_U$	Relative to the upper stream
$_{up}$	Relative to the upper wall of an inlet channel
$_s$	Relative to stochastic motion

Superscripts:

$\_^{ext}$	At extinction
$\_^{ign}$	At ignition
$\_^{st}$	Steady state
$\_^{wall}$	At the wall

Abbreviations/Acronyms:

CFD	Computational Fluid Dynamics
LDV	Laser Doppler Velocimetry

LES4LPP	Large-Eddy Simulations for Lean Premixed Prevaporised (combustion)
LPP	Lean Premixed Prevaporised
MOLECULES	Modelling of Low Emission Combustors using Large-Eddy Simulations
ORACLES	One Rig for Accurate Comparisons with Large-Eddy Simulations
rms	Root mean square
RQL	Rich Quench Lean (burn)
SDA	Semi-Deterministic Approach

1. Introduction

The development of systems of aeronautical propulsion able to meet the forthcoming drastic certification requirements on the reduction of the level of pollutants emission heavily relies on the development of new concepts of combustion chambers based on or combining rich-quench-lean (RQL) or lean-premixed-prevaporised (LPP) technologies [1]. If one focuses on the latter type of approach, the development of reliable LPP systems lies in the capability of preventing the occurrence of destructive and/or undesired phenomena *a priori* present in these systems such as auto-ignition during the mixing stages between fuel and hot air, and extinction or flashback that might appear particularly during rapid transient engine regimes. Among others, the kerosene injection system has to be optimised in order to yield a premixed prevaporised combustion zone as homogeneous as possible. Unfortunately, in such a system, it is well known that the mixing between the hot air and the vaporised fuel can not be perfect because of the risk of auto-ignition that can occur in the mixing device. Consequently, the gaseous mixture in the combustion chamber may feature spatial inhomogeneities of its equivalence ratio field [2,3] that may compromise the targeted objective in terms of pollutants emission reduction and also complicate the control of the flow stability. Accordingly, the success in designing an efficient and reliable LPP system requires to supplement the existing know-how related to more "traditional" designs with additional investigations based on both experiments and numerical simulations of simplified reactive flows configurations but still featuring most of the prominent phenomena of the real system such as flashback and extinction susceptibility and large scale unsteadiness related properties. Concerning the aforementioned specificity of LPP based systems, the large-eddy simulation (LES) appears to be the best suited modelling approach because of its ability to capture most of the relevant flow properties such as second-order correlations controlling the turbulent transports and combustion features as well as the large scale flow unsteadiness properties [4]. Regarding the latter point, the capability of discriminating, from an experimental point of view, between the respective contribution of the coherent motion (often acoustically driven) and of the turbulence to the flow dynamics appears

to be highly desirable in order to assess in depth the performances of LES. In the late 90's, a test facility named ORACLES (**O**ne **R**ig for **A**ccurate **C**omparisons with **L**arge-**E**ddy **S**imulations) has been designed and developed in the framework of a European research programme LES4LPP by Besson et al. [5] with the primary and specific long-term objective of progressively building up an experimental database adapted and useful for the test of modelling of LPP flows configurations by a LES based approach (although RANS based simulations can also be tested, see for instance Kurenkov and Oberlack [6]). Nguyen and Bruel [2] and Nguyen [3] have pursued this objective in the framework of the European programme MOLECULES [7] aimed at promoting the extensive use of LES to model low emissions combustors. Since the resulting experimental database proves already to be particularly valuable in the context of the test of LES modelling as it is evidenced by its use in the recent numerical studies by Domingo et al. [8], Duwig et al. [9], Duwig and Fureby [10] and Duwig [11], the primary objective of the present contribution is to shed light on the main features of the flow fields corresponding to this database and concurrently, draw attention of the CFD community to the availability and usefulness of such a flow configuration for benchmarking activities. The first part of the database, presented in the present contribution, consists of data characterising the lean extinction and velocity field properties. In a future phase, the present database should be supplemented by additional measurements aimed at characterising the scalar field (temperature and species). It is worth noticing that there exists a series of well documented TNF (Turbulent Non-premixed Flames) databases which focuses actually on the diffusion and partially premixed flames such as simple jet flames, piloted jet flames, bluff-body stabilised jet flames and swirl-stabilised flames [12]. The ORACLES database complements TNF databases in terms of the progression of complex confinement geometries and combustion modes. The ORACLES geometry can permit to feature simultaneously momentum/scalar mixing layers, shear layers and recirculating flows.

Regarding combustion modes, fully premixed or partially premixed (or stratified) combustion regimes can be considered on the ORACLES burner.

After rapidly introducing the different aspects related to the test facility, flow parameters, metrology and data processing, the extinction characteristics are first presented. Then, some examples of flame visualisations in direct light are presented. Finally, the main properties of the velocity field are discussed for the different flow configurations investigated. The three different reacting flows situations have been chosen to feature a progressive stratification at the injection while keeping constant the same thermal output. Thus, turbulent combustion models able to deal either with partially premixed (or stratified) or solely with fully premixed reacting flows can be tested along with the whole spectrum of turbulence models. In that respect, examples illustrating the recourse to an ad-hoc triple decomposition of the instantaneous velocity signal help in discriminating between the contribution of the deterministic motion (if present) and of the turbulence to the velocity dynamics and are thought of as being particularly useful in the context of the test of LES simulations or more generally, unsteady simulations.

2. Experimental configuration and metrology

2.1. The ORACLES test rig

The test rig ORACLES has been described in details elsewhere [2,3,5] and thus only a brief description will be given hereafter. The rig is made of four main sections, namely: 1) two mixing chambers, 2) a long section of constant rectangular cross section required to obtain two fully developed turbulent channel flows, 3) a unique combustion chamber with thermally insulated walls where the combusting zones are stabilised at the entrance by a symmetric sudden expansion and 4) an exhaust section. Figure 1 presents a schematic view of the whole test rig and the detailed geometry at the sudden expansion. It is additionally noted that the reaction zones are formed by the two flame brushes stabilised in the shear layers formed by the

step corners and that the flame brushes are interacting with the wake generated by the trailing edge of the splitter plate which initially seperates the two streams. The fuel (commercial propane) and the air supplied to the two inlet channel flows from high-pressure storage reservoirs are premixed and homogenised in two separate settling chambers.

[LOCATION of FIGURE 1]

2.2. Flow parameters, metrology and data processing

The different labels and parameters that characterise the different flows are listed in Table 1. Flow nc_1 is the non-combusting "reference" flow whereas the reacting flows c_1, c_2 and c_3, featuring the same thermal power output, differ only by their inlet equivalence ratio difference between the two feeding streams that ranges between 0 (flow c_1) and 0.20 (flow c_3). In the latter case, such an equivalence ratio difference leads to very different intrinsic laminar flame properties with for instance a related laminar flame speed ratio of around three between the leaner and the richer reactants streams. The bulk velocity of the incoming streams is of the order of U_{bulk} = 11.0 m/s. The Reynolds number estimated from U_{bulk}, the height of each inlet channel H = 30.4 mm and the kinematic viscosity of fresh mixture at the reference temperature T_0 = 276 K, is of the order of 25000. During the course of the experiments, five gas sampling and chromatographic analyses have been carried out to determine accurately the average composition of the commercial propane used as fuel. The resulting average composition (in volume) proved to be as follows: 2.23% C_2H_6, 8.51% C_3H_6, 86.39% C_3H_8, 0.30% C_4H_8, and 2.57% C_4H_{10}. The corresponding global formula $C_{3.01}H_{7.85}$ is very close to that reported by Besson et al. [5]. The mean wall pressure measurements in the inlet channels were carried out by using a Kimo probe (type CPN1-0SV, range –300 to +700 Pa) coupled with a selection box FCO91MK2 that scrutinised successively the twenty pressure taps fitted on both inlet channels wall. The velocity measurements were performed using a hardware similar to that of Besson et al. [5] except for the additional probes required for two-point measurements. A system

consisting of a Spectra 2017 four-beam two-color laser coupled with one (one-point two-component measurements) or two (two-point one-component measurements) Dantec fiber probes operated in a backward-scattering mode and preamplified photomultipliers was used. The ellipsoidal probe volumes had a large diameter of roughly 4 mm and a small diameter of 0.2 mm. The depth of field of the photomultipliers was 0.4 mm. The flow was seeded with micron-sized SiO2 and TiO2 particles. The analogic signal was sent to and processed by two Dantec burst spectrum analysers (type 57N21) before being sent via an IEEE 488 interface to a computer for storage and post-processing. The laser probes were displaced by a three-step by step motor based traversing system. The various processes (acquisition, storage, probe displacement, data processing) were controlled by an in-house LabVIEW based program. All the velocity measurements were realised in the vertical midspan plane $z = 0$ of the test rig at eleven different x stations: two in the inlet channels (x=-5h and -5.8h), one at the dump plane (x=0h) and eight in the combustor (x=1h, 2h, 3h, 4h, 7h, 8h, 9h, and 10h). For quantities requiring measurement in time coincidence, namely the shear stress at one point or a two-point one-velocity component correlation, the two burst spectrum analysers were operated in a mode combining a master-slave setup for the time initialisation followed by a private-private mode for the data acquisition. Then, a post-synchronisation data process was performed to validate the measurements in coincidence. The processing of the data contained in the database gives access in particular to i) the mean streamwise and normal components of the velocity and their related *rms* fluctuations, ii) the shear stress, iii) the spectra of the velocity fluctuations, iv) the histogram of the velocity components. In the examples of results presented below, the statistical bias of the measured velocity towards higher values was corrected by the sample and hold technique [13] by using the inter-arrival time as weighting factor. To get meaningful and converged statistics, the number of instantaneous values to acquire and process at each measurement point varied between 2048 for the mean velocity components to 10240 for the spectra and the shear stress (acquired in ten separate blocks of 1024 values each). The spectra presented hereafter are calculated by reconstructing an evenly sampled signal using a linear

interpolation on each block, performing a fast Fourier transform and averaging the resulting ten spectra. Finally, simultaneous two-point one-component velocity measurements were realised to investigate the correlation between the two velocity streamwise components measured at a fixed point on the axis of the upper inlet channel (Point A, x=-5h, y=2.86h) and at points located crosswise in the lower inlet channel at x=-5h and at the dump plane x=0. The availability of the raw data allows for a direct calculation of the random errors associated to the LDV acquisition. In the following, they are estimated by determining a 95% confidence interval using the formulas given by Benedict and Gould [14]. From the characteristics of the incoming streams (composition and turbulence characteristics), one can quantify some important combustion characteristic numbers such as Damköhler number $Da = \Lambda_t / \tau_c$ and Karlovitz number $Ka = \tau_c / \tau_K$ where Λ_t, τ_c and τ_K are the integral, chemical and Kolmogorov time scales, respectively. The results calculated are reported in Table 1. Also presented in the same table are the estimates of the Taylor (λ_x) and Kolmogorov (η_K) length scales that are helpful for choosing an appropriate LES grid. The combustion regimes can be then reasonably assumed to be close to those prevailing in the vicinity of the "frontier" between the thickened-wrinkled flamelets and the corrugated flamelets domains [15].

[LOCATION of TABLE 1]

Since Besson et al. [5] have shown that quite a vigorous pulsating mode could be present in this type of flow, the velocity data signals have been processed accordingly by systematically using the triple decomposition proposed originally by Hussain and Reynolds [16,17]. Accordingly, whenever relevant, the instantaneous velocity signal $u_i(t)$ has been decomposed into three parts e.g. $u_i(t) = \overline{u}_i + u_i'\big|_p(t) + u_i'\big|_s(t)$. In the latter expression, $\overline{u}_i$ denotes the time-average value, $u_i'\big|_p(t)$ stands for the periodic coherent motion and $u_i'\big|_s(t)$

represents the stochastic fluctuation. Processing the experimental data accordingly gives access to the phase average defined by $< u_i > (t) = \bar{u}_i + u_i' \big|_p (t)$. The multi-step procedure used to perform this triple decomposition on the discrete signal $u(t)$ provided by the LDV is described below:

1. Straightforward time averaging procedure to determine $\bar{u}$.

2. Calculation of the Fourier transform of the total fluctuating velocity $u'(t)$: $FT_{u'}(f) = R(f) + iI(f)$.

3. Calculation of the energy density spectrum *(EDS)*: $EDS(f) = \left(R^2(f) + I^2(f)\right)/\Delta f$ where Δf denotes frequency resolution.

4. Detection in the *EDS* local maxima $f_{\max} = f_p$ (if any) associated to the periodic motion by absolute comparison of all *EDSs* in the spectrum or application of a detection criterion i.e. $EDS_{\max} = 5\overline{EDS}$ where $\overline{EDS}$ is the averaged *EDS* of the ten neighbouring points around the investigated point.

5. Definition of the two cut frequencies: $f_{cut1}, f_{cut2} = f_{\max} \pm 5\Delta f$, that delimitate the peak.

6. "Removal" of the coherent peak between f_{cut1} and f_{cut2} and interpolation of the remaining spectrum in the defined "hold" to obtain the energy density spectrum EDS_s associated to the stochastic motion only.

7. Calculation of the transfer function $H_s(f) = \left(EDS_s(f)/EDS(f)\right)^{1/2}$ and then calculation of the inverse Fourier transform of the product $H_s(f) * FT_{u'}(f)$ to get $u_s'(t)$.

8. Calculation of the periodic part of the motion by $u_p'(t) = u'(t) + u_s'(t)$.

3. Results and discussion

3.1. Lean extinction properties

When developing LPP combustors, the determination of extinction characteristics is one essential phase to establish correctly the stability margin of the system. Thus, this kind of determination has been carried out on the ORACLES rig in order to permit the test of the capability of the numerical simulations to predict accurately the conditions of occurrence of such a phenomenon. The lean flammability limits have been sought over a wide range of extinction configurations corresponding to four generic situations.

In Situation 1, the two incoming streams are reacting and possess the same mass flow rate. The extinction of the upper stream was sought while the lower stream was kept reacting at an equivalence ratio Φ_L^{st}. The influence of the mass flow rate and of Φ_L^{st} on the extinction characteristics of the upper stream (*i.e.* on Φ_U^{ext}) was investigated. Situation 2 differs from Situation 1 by the fact that the lower stream is not burning anymore since it is fed only with air. Situation 3 is similar to Situation 1 except that in this case, this is the simultaneous extinction of both streams which is sought. Situation 4 scenario is similar to that of Situation 1, except for the mass flow rates which are now different between the two streams, with $Q_U < Q_L$. The idea behind this was to detect if the presence of a momentum mixing layer between the two streams (instead of that of a wake as it was the case in Situation 1) was influencing the values of Φ_U^{ext}.

In all situations, the methodology employed was quite similar. For instance, in Situation 1 with $\Phi_L^{st} = 0.65$, the following scenario was used:

Step 1: Setting of the two air streams at the targeted mass flow rate.

Step 2: Descent of the spark plug behind the upper step, opening of the gas line of the upper stream and ignition as soon as $\Phi_U^{ign} = 0.75$. Removing of the plug.

Step 3: Opening of the gas line of the lower stream and auto-ignition at $\Phi_L^{ign} = 0.75$.

Step 4: Stabilisation of the two reacting zones at $\Phi_U^{st} = \Phi_L^{st} = 0.65$ during one minute and plunging in complete darkness the hall hosting the rig.

Step 5: Progressive closing of the gas valve aperture of the upper stream, in a quasi-steady way, until extinction is eventually observed by a human observer placed by the test rig.

Considering the regulation system and the fine control of the operational conditions, the systematic error in equivalence ratio associated with the above methodology and gas analyser characteristics is estimated to be equal to ±0.02.

For the sake of conciseness, Table 2 lists only the range of parameters differentiating the various configurations as well as the value range at which the one-stream (Situations 1, 2 and 4) or the two-stream extinction (Situation 3) was observed. The values obtained for each individual case can be found in the database itself.

In Situation 1, a weak dependence of the values of equivalence ratio at extinction of the upper stream on a variation of the Reynolds number is obtained. A very slight decrease of Φ_U^{ext} can be noted though when Re increases. The diminution of Φ_U^{ext} with increasing Reynolds number can be reasonably attributed to the heating of the combustor walls due to the related increase of the heat load during the test. A similar trend was observed by Korusoy and Whitelaw [18]. Varying Φ_L^{st} between 0.60 and 0.75 for $\mathrm{Re}_L = \mathrm{Re}_U$ ranging from 25000 up to 65000 shows that, for a given Reynolds number, Φ_U^{ext} is quasi-independent of Φ_L^{st}. Moreover, we still recover the fact that, for a given value of Φ_L^{st}, Φ_U^{ext} is quasi-independent of the value of the Reynolds number. In Situation 2, a weak sensitivity of the value of the equivalence ratio at extinction of the upper stream to the variation of the Reynolds number is also observed, with a marginal decrease of Φ_U^{ext} when Re increases. These results are coherent with those obtained by De Zilwa et al. [19] for one-stream dump expansions. In Situation 3, Φ_U^{ext} and Φ_L^{ext} are extremely close one from each other. There was always one stream which was extinguishing first, quickly followed by the other. In some situations, prior to the extinction of the first stream, it was observed that the two reaction zones were oscillating longitudinally in phase opposition.

The values of Φ_U^{ext} obtained here are very close to those obtained in the corresponding one-stream extinction configuration *i.e.* in Situation 1. Finally, in Situation 4, Φ_U^{ext} proved to be quite independent of both Re_U and $\mathrm{Re}_L - \mathrm{Re}_U$. One can conclude that 1) the mechanism of stabilisation of flames is not sensitive to the instabilities developing within the mixing layer and 2) the presence of a developing wake or a momentum mixing layer (Situation 4) around the (y=2.18h)-plane does not affect the shear layers developing at the level of the steps corners sufficiently early to influence significantly the stabilisation of the two flame brushes.

In conclusion of this section, it can be said that the values of the equivalence ratio at which the extinction of the reacting zones occurs are almost independent of the Reynolds number of the incoming flow and from the scenario of extinction considered (one or two-stream extinction, wake or mixing layer developing from the trailing edge of the splitter plane) and that all the recorded values belong to the interval 0.54±0.030. It will be interesting to see if the related numerical simulations will be able to reproduce such a behaviour.

3.2. Combustion zone visualisations

Some examples of flame visualisations in direct light are presented in Figure 2 to provide a clear illustration of the morphology of both the mean and the instantaneous reacting flows investigated. Although these visualisations correspond to a spanwise integration of the combustion zone and the lean side flames are not easily visible (especially for flow c_3), they nevertheless permit to realise that the mean flow structure is far from being representative of the instantaneous states explored by the flow. Indeed, compared to the mean flow pattern obtained with a time exposure of 1/50s, the instantaneous realisations of the flow obtained by reducing the time exposure down to 1/500s exhibit a periodic sequence of morphologies that can be associated to a flapping of the two anchored flame brushes. In case c_1, the flapping seems to be quite symmetric with respect to the combustor centreline whereas for flows c_2 and c_3, there exists a certain dissymmetry of the flow structure induced by the flow stratification.

[LOCATION of FIGURE 2]

3.3. Velocity field properties

The mean-flow field properties of the different flows considered are first presented. Then, the respective contribution of the coherent and stochastic motions to the energy of the velocity fluctuations is determined in each case. Finally, the results of the simultaneous two-point one-component velocity measurements will be given.

3.3.1. Main properties of the mean velocity field

In the inlet channels

Figure 3 presents the profiles, obtained at x=-5h, of the mean streamwise and transverse velocities and of the corresponding *rms*-velocity fluctuations normalised by the bulk velocity. These profiles were realised with a high spatial resolution ($\Delta y = 0.1\,\mathrm{mm}$) and the probe measurement volume was approached to less than 0.15mm off the wall for the longitudinal velocity component. The profiles of $\overline{u}/U_{bulk}$ (Figs. 3.a and 3.b) are typical of those of a fully developed turbulent channel flow with a maximum reduced streamwise velocity of 1.3 to 1.4. For a given inlet channel, no noticeable difference between the profiles measured for the different reacting flows is observable. One might note a slight deficit when comparing the velocity profiles of the three reacting flows to those obtained for the equivalent non-combusting flow nc_1 particularly for the upper stream (Figs. 3.a). In addition, all the velocity profiles are quite equivalent between the two inlet channels. The profiles of $\overline{v}/U_{bulk}$ (Figs. 3.c and 3.d) are also all quasi-similar regardless of the flow considered and are close to the expected value $\overline{v} = 0$. However, one notes a minor but systematic shift towards negative values with an amplitude of approximately 1% of the bulk velocity. For the streamwise *rms*-velocity fluctuations (Figs. 3.e and 3.f), if the inert flow is characterised by a maximum value of an order

of $0.2U_{bulk}$ associated to the parietal shear, the reacting flows exhibit an important augmentation of these velocity fluctuations with the highest level of u' reached for flow c_2. Contrary to what is observed for the streamwise *rms*-velocity fluctuations u', the amplitude of the transverse *rms*-velocity fluctuations v' remains of the same order of magnitude for all four cases (Figs. 3.g and 3.h). One might conclude here that, although the global thermal power output of the three reacting flows is the same, the presence of the initial equivalence ratio gradient may result in significantly larger fluctuations of the streamwise velocity in the feeding channel flows. Thus, the prescription of the inflow boundary conditions of any related numerical simulations should be carried out with such a behaviour in mind.

[LOCATION of FIGURE 3]

At the dump plane

The velocity field mesurements were performed at the dump plane with a high spatial resolution and the resulting profiles are shown in Figure 4. The profiles of $\overline{u}$ appear to be perfectly symmetric with respect to the centreline of the test rig (*i.e.* at y=2.18h) irrespective of the flow investigated. The profiles of $\overline{u}$ obtained for the different combusting flows are nearly superimposed and one might again note a marginal deficit compared to the profile of $\overline{u}$ obtained for the inert flow nc_1 (Figs. 4.a and 4.a'). The profiles of $\overline{v}$ in the uniform reacting flow c_1 and in the inert flow nc_1 are close one from each other whereas the results prove to be quite different regarding the initially stratified reacting flows c_2 and c_3 (Figs. 4.b and 4.b'). The double peak of energy on the profile of u' associated to the wake developing from the trailing edge of the splitter plate, observed for the inert flow nc_1, is almost absent for all three reacting flows due to an important augmentation of the energy level due to the appearance of a periodic motion (Figs. 4.c and 4.c'). For each reacting case, the crosswise distribution of the streamwise velocity fluctuations u' is found to be symmetric relative to the centreline of the test rig.

However, in contrast to the results obtained in the feeding channel flows, one can note here a sensitivity of the profiles of v' to the equivalence ratio of the incident stream with a higher level of the fluctuations at the lower side (richer reactants streams) than that at the upper side (leaner reactants streams) (Figs. 4.d and 4.d').

[LOCATION of FIGURE 4]

In the combustion chamber

Figures 5 and 6 show the results for the time-averaged streamwise and transverse velocities as well as the corresponding *rms*-velocities at eight streamwise locations downstream of the dump plane for all the flows studied. Let us first consider the non-combusting flow nc_1. The profiles of $\overline{u}$, particularly from x=7h onwards, are found to be asymmetric relative to the centreline of the test rig (Fig. 5.a). Such a tendency was also reported by Besson et al. [5]. This finding is also in accordance with that of Abbott and Kline [20] who observed that, for a geometric expansion ratio A_r>1.5 (A_r=1.84 for the ORACLES rig), the mean flow became asymmetric. Thus, the flow deflects towards the lower wall of the combustor yielding consequently a lower recirculation zone shorter than the upper one with a reattachment length observed at x=5.5h whereas the upper recirculation zone extends to x=8.0h (Table 3). The recent simulations by Duwig et al. [9] of the present flow configuration confirm the presence of such a dissymmetry and its sensitivity to the expansion ratio value. If one defines now the potential cores of the jet as the regions where the mean streamwise velocities are within 15% of the maximum inlet velocity, two potential core regions are found to be situated around y=1.51h and y=2.86h for flow nc_1, persisting until approximately x=4h and exhibiting the lowest streamwise *rms*-velocity fluctuations, of the order of $0.1U_{bulk}$ (Fig. 6.a). Not surprisingly, the maximum values of u' and v' (Figs. 6.a, 6.a', 6.e and 6.e') are found in the shear layers between the high-velocity potential cores and the low-velocity recirculation zones and

correspond to the inflection point in the mean-velocity profiles of $\overline{u}$ (Fig. 5.a). In addition, the two local maxima of u' and v' (around y=2.18h), corresponding to the interaction between the wake of the splitter plate and the two incident streams, are observed until the streamwise station x=4h (Figs. 6.a and 6.e). As one travels further downstream, the flow relaxes progressively towards the structure of a fully developed turbulent channel flow but it is still slightly asymmetric at the downstream distance of x=10h, with the measured centerline velocity of around $0.89U_{bulk}$ being consistent with the geometric expansion ratio of the test rig *i.e.* A_r=1.84. It is worth noticing that the profiles of $\overline{v}$ are already re-homogenised transversely at a streamwise distance of x=10h (Fig. 5.e').

[LOCATION of TABLE 3]

[LOCATION of FIGURE 5]

[LOCATION of FIGURE 6]

When combustion is present and for the homogenous reacting flow c_1, one notes firstly the symmetry of the profiles of $\overline{u}$ associated to the anti-symmetry of the profiles of $\overline{v}$, with respect to the centreline of the rig (Figs. 5.b, 5.f and 5.f'). The two mean recirculation zones are much shorter than those observed in the inert case nc_1 since the measured reattachment lengths (similar for both zones) are found to be equal to 2.3h (Table 3). Such a shortening is the direct consequence of the strong and symmetric flow acceleration due to the burnt gas expansion. One observes in Figures 6.b' and 6.f that the fields of the velocity fluctuations u' and v' can feature much higher levels than those obtained in the inert case, with values of u' reaching $0.4U_{bulk}$ in the far field (x=9h, 10h) or values of v' larger than $0.2U_{bulk}$ in the near field (x=1h). However, it is worth noticing that the velocity fluctuations u' and v' in the inert case nc_1 (Figs. 6.a and 6.e) always exhibit important amplitudes particularly in the near field (around $0.22U_{bulk}$ and

$0.16U_{bulk}$ for u' and v', respectively) at the locations y=1h and y =3.37h corresponding to the development of the lower and upper shear layers.

As far as the two reactive flows c_2 and c_3 are concerned, their incoming stratification results in the expected dissymmetry of the mean flows as shown by the profiles presented in Figures 5.c and 5.d. The recirculation zones sizes decrease with increasing equivalence ratio due to the stronger flow acceleration associated to the local higher thermal expansion. Thus, for flow c_2, the lower (rich side) and upper (lean side) recirculation zone lengths are equal to 2.3h and 2.5h, while for flow c_3, these values amount to 1.9h and 2.8h, respectively (Table 3). The anti-symmetric behaviour of the profiles of $\overline{v}$ with respect to the combustor centreline is no longer observed here when compared to the homogeneous reacting flow c_1. Indeed, the inlet equivalence ratio stratification strongly affects the transverse velocity field with quite an important negative values of $\overline{v}$ at the lower (rich) side, indicating a noticeable mean flow deflection towards the bottom wall of the test rig (Figs. 5.g, 5.g', 5.h and 5.h') which results in a non-zero $\overline{v}$ value on the centreline of the test rig. Regarding the streamwise *rms*-velocity fluctuations u' and as shown in Figures 6.c, 6.c', 6.d and 6.d', the two reacting flows c_2 and c_3 behave in quite a similar fashion, with an important amplitude of the velocity fluctuations in the vicinity of the walls and a slight wrinkling of the ensemble of the profiles. As for the transverse *rms*-velocity fluctuations v' (Figs. 6.g, 6.g', 6.h and 6.h'), between the profiles that can be described as a double-hump pattern for flow c_2 (one hump close to each wall) and the profiles that are roughly three-hump shaped for flow c_3 far downstream (x=9h, 10h), one can simply indicate that, unlike what is observed for flow c_1, there is a clear change of the morphology between the profiles measured in the near and in the far fields.

3.3.2. Deterministic vs. stochastic contributions to the velocity field dynamics

In the inlet channels

In Figure 7, we present the energy density spectra (EDS) of the streamwise velocity fluctuations obtained at x=-5h and on the axis of each of the two channels, *i.e.*, at y=1.51h and 2.86h, for all the investigated flows. The spectra obtained for the three combusting flows (c_1, c_2 and c_3) exhibit a distinctive peak of energy at a fundamental frequency of approximately 50Hz that is absolutely absent in the spectrum obtained for the non-combusting flow nc_1. Such a presence is specific to the combusting flows. One notes also a replica, much less energetic though, at a frequency value around 100Hz. Apart from this remarkle frequency characteristics, all the spectra take the form of a quasi-flat plateau low-frequency region (up to about 100Hz) followed by a -5/3 power-law decay in the high frequency part, a behaviour commonly found in equilibrium turbulence. Since no peak of energy is observed on the corresponding spectra of the transverse velocity component [3], it is clear that the incoming flows are exhibiting a piston-like streamwise pulsation which represents quite a challenge to deal with as far as simulations are concerned. As a matter of fact and even in the most recent simulations of these flows by Domingo et al. [8], Duwig and Fureby [10] or by Duwig [11], this pulsation is not yet predicted by the simulations but is instead emulated at the inlet boundary by injecting in the prescribed time varying velocity streamwise component a periodic signal at the measured frequency.

[LOCATION of FIGURE 7]

The probability density functions (PDF) associated with the streamwise velocity component are calculated at the same locations as for the energy density spectra presented in the preceding paragraph and the results are presented in Figure 8 along with the values of the skewness (S) and flatness (F) factors, defined by $S = \overline{u'^3} / \left(\overline{u'^2}\right)^{3/2}$ and $F = \overline{u'^4} / \left(\overline{u'^2}\right)^2$, respectively. The difference between the shapes obtained for flow nc_1 and for the reacting ones is evident. In the latter cases, the instantaneous velocity range is much wider starting from less than 10m/s to more than 20m/s while for flow nc_1 all the values fall between 13m/s and 17m/s.

Unlike what is observed for flow *nc₁*, the PDF shapes for the reacting flows significantly depart from the Gaussian form with a slight but visible bimodal character that can be associated to the presence of the coherent periodic motion. Indeed, if one considers a coherent motion of the form $u_p^{'}(t) = A\sin(2\pi f t)$ (here typically $f \approx 50Hz$) where A designates its amplitude, the corresponding PDF of such a signal is given by $P(u_p^{'}) = \frac{1}{\pi\sqrt{A^2 - u_p^{'2}}}$ [21] which possesses two asymptotic peaks for $u_p^{'} \to \pm A$. Thus, as soon as in the velocity fluctuations, the coherent motion begins to appear, the PDF shape will begin to exhibit some bimodal feature more or less pronounced, depending on the relative level of the contribution of that particular motion.

[LOCATION of FIGURE 8]

By using the semi-deterministic approach, the large scale unsteadiness of the flow can be carefully identified and its contribution to the flow field dynamics can be estimated. Figure 9 displays the profiles versus the reduced coordinate y* of the total u', stochastic u'_s and periodic u'_p streamwise *rms*-velocity fluctuations as well as those of the relative contribution Eu'_p of the periodic motion to the total energy of the fluctuations. It is observed in Figs. 9.a and 9.e that the amplitude of the total *rms*-velocity fluctuations is much larger for the reacting flows *c₁*, *c₂* and *c₃* than for their inert counterpart *nc₁*. In both channels, the *rms* values for flow *c₃* are slightly larger than for flow *c₁* and markedly smaller than for flow *c₂*. It is clear from the results plotted in Figs. 9.b and 9.f that the contribution of the sole stochastic motion at x=-5h is not modified by the presence of combustion in the test section. In addition, the contribution of the periodic motion is equivalent in the two channels and is more important in cases *c₂* and *c₃* than in case *c₁* (Figs. 9.c and g). This leads us to conclude that the increase of the level of the streamwise *rms*-velocity fluctuations is only due to the appearance of a strongly energetic

periodic motion. This coherent motion is most dominant in the centreline of each channel and less vigorous close to the walls due to the viscous damping and it can contribute to more than 90% of the total energy of the streamwise velocity fluctuations, regardless of the presence of an equivalence ratio difference (Figs. 9.d and 9.h). Unlike what is observed for the stochastic motion, the coherent motion proved to be sensitive to the stratification of the two incoming streams with flow c_2 featuring an absolute maximum level of u'_p nearly 50% higher than that recorded for flow c_3. It is additionally noted that such a pulsating behaviour of the reacting flows, corresponding to a vigorous oscillation of the phase-velocity, is *a priori* an element favouring the possibility of flashback in the feeding channels, which was not observed here due to the fact that the minimum values of the phase-average velocity [2,3] are still significantly larger than that of the premixed turbulent flamme considered.

[LOCATION of FIGURE 9]

The simultaneous presence of turbulence and of the periodic motion in the inlet channel flows is obviously a source of difficulty when trying to simulate this sort of flow and more specifically to prescribe the (time varying) velocity boundary conditions. As mentioned previously, all the related LES simulations of the present flow configurations rely so far on the direct injection of the periodic motion (at the measured frequency) at the inlet boundaries. This being done, one is left with the question of prescribing a boundary condition that permits also to take into account the presence of the turbulent fluctuations. In that respect, Duwig and Fureby [10] and Duwig [11] used the digital filtering proposed by Klein et al. [22] whereas Domingo et al. [8] carried out preliminary channel flow simulations whose ouput was subsequently used to generate the turbulent velocity fluctuations at inlets. Other alternative ways could certainly be chosen thanks to the availability of the raw data (*i.e.* instantaneous values and corresponding time) in the present database. For instance, the prescription of the turbulent velocity fluctuations

at the inlet section could be based on the proposal by Biferale et al. [23] who suggested to mimic a turbulent signal by solving a stochastic differential equation based on a Langevin equation modified to ensure a -5/3 power decay of the spectrum of the generated signal. In such an approach, the input parameters are the *rms*-velocity fluctuations and the integral time scale. With the present database, these two parameters can be easily extracted from the measurements by performing the triple decomposition of the measured instantaneous velocity signal. Then, the time auto-correlation function of the sole stochastic fluctuations can be calculated and integrated to yield the desired temporal integral length scale of the stochastic fluctuations. To illustrate this, Figure 10.a presents the normalised auto-correlation function of the total streamwise velocity fluctuations recorded at point (x=-5.8h, y=1.51h) for the reactive case c_1. As previously mentioned, its periodic behaviour is due to the piston like pulsation of the flow which yields the harmonic velocity fluctuations $u'_p(t)$ whose auto-correlation function is obviously periodic (Fig. 10.b). Once the periodic motion has been filtered out, the auto-correlation function of the sole stochastic contribution (Fig. 10.c) which, as expected, relaxes towards 0 for large time lag, permits to calculate the required time integral length scale at this point ($\Lambda_t = 1.23 ms$ in that case).

[LOCATION of FIGURE 10]

At the dump plane

The energy density spectra, in particular, of the only transverse velocity component measured on the axis of the feeding channels (y=1.51h and 2.86h) and on the combustor centreline (y=2.18h) are displayed in Figure 11. It is observed that the energetic peak appears to be more vigorous on the side of the richer reactants streams (Figs. 11.h and 11.i). In the homogeneous reacting flow c_1, the spectrum calculated on the centreline of the test rig exhibits no energetic peak (Fig. 11.d) because in that case, the flapping of the flame fronts is symmetric

with respect to the centreline. This is no longer the case for flows c_2 and c_3, for which a peak of energy appears on the spectra obtained on the centreline of the combustor and the bigger the equivalence ratio difference, the higher the energetic peak (Figs. 11.e and 11.f). This is the signature of the asymmetry of the flapping of the flame fronts developing downstream of the dump plane and observed on the flame visualisations (Fig. 2).

[LOCATION of FIGURE 11]

Figure 12 depicts the various profiles of the streamwise and transverse velocity fluctuations and of the relative contribution of the periodic coherent motion to the total streamwise and transverse velocity fluctuation energy. It is observed on the profiles of the total streamwise *rms*-velocity fluctuations (Fig. 12.a) that the double peak of energy associated to the wake of the splitter plate is nearly absent in the combusting flows c_1, c_2 and c_3 in comparison to what is observed for the non-combusting flow nc_1. This double peak reappears slightly though on the profiles of the stochastic fluctuations (Fig. 12.b). For the three reacting flows, one finds out that all the profiles of u'_s and v'_s are nearly superimposed (Figs. 12.b and 12.f). It is worth noticing that the periodic fluctuations of the streamwise velocity u'_p behave in a way similar as that observed in the feeding channel flows (Fig. 12.c) whereas the periodic fluctuations of the transverse velocity v'_p prove to be highly sensitive to the nature of each incident flow (Fig. 12.g). Indeed, for the initially stratified reacting flows c_2 and c_3, the amplitude of the *rms* values of v'_p at the richer reactants streams (*i.e.*, lower side) is significantly larger than that at the leaner reactants streams (*i.e.*, upper side). It has thereby a dramatic influence on the crosswise distribution of Ev'_p, for instance in case c_3, the maximum contribution of Ev'_p can attain 70% at the side of the richer stream against only 20% at that of the leaner one (Fig. 12.h).

[LOCATION of FIGURE 12]

In the combustion chamber

Figure 13 presents the fields of the relative contribution of the coherent periodic motion at the dominant fundamental frequency of around 50Hz to the local total energy of the streamwise (Eu'_p) and transverse (Ev'_p) velocity fluctuations. The piston-like type motion in the feeding channels flows is clearly visible in the combustor and in the vicinity of the dump plane. This kind of behaviour occurs only for the streamwise component of the velocity. For flows c_1, the fields of Eu'_p and Ev'_p are quite symmetric relative to the combustor centreline, namely at y=2.18h and the quasi-zero contribution of Ev'_p is clearly observed along this location. As a progressive stratification is introduced at the injection, the morphology of the cartographies are modified, particularly that of Ev'_p. For the most unstable pulsating flow *i.e.* flow c_2, a very important periodic fluctuation at the flame anchoring position is observed.

[LOCATION of FIGURE 13]

3.3.3. Simultaneous two-point one-component velocity measurements

As far as the simulations of such flows are concerned, evidencing experimentally the presence of a coherent longitudinal flow motion in the inlet channels and quantifying its contribution are important but not sufficient to permit a proper setting of the boundary conditions. Indeed, information regarding the phase angle between the coherent motions in the two channels is needed. Thus, simultaneous two-point one-component (streamwise) velocity measurements were carried out. One of the two points, point A was located on the centreline of the upper channel (x=-5h, y=2.86h) and kept fixed while the second point (corresponding hereafter to index y), was selected at different y-locations at x=-5h in the lower inlet channel and at the

dump plane. The resulting normalised correlation coefficients $Ru'_A u'_y$ are then displayed in Figure 14. The total velocity fluctuations obtained at point A are found to be strongly correlated with those obtained at the points situated crosswise at station x=-5h in the lower inlet channel (Figs. 14.a, 14.b and 14.c). After extraction of the coherent motion, it turns out that, as expected and for all reacting flows, the stochastic fluctuations are not correlated and that the observed correlation of the total fluctuations comes uniquely from the coherent periodic motions in the two channels which proved to be correlated almost perfectly in phase, with a correlation coefficient practically equal to 1. This in-phase inlet pulsation characteristics is also observed at the dump plane (Figs. 14.d, 14.e and 14.f) without any remarkable difference between the three reacting flows.

[LOCATION of FIGURE 14]

4. Concluding remarks

The results contained in the present experimental database show that:

- The values of the equivalence ratio at which the lean extinction of the reaction zones occurs are almost independent from the Reynolds number of the inlet flow and from the extinction geometry considered. The recorded values of the equivalence ratio at extinction belong to the interval 0.54±0.030.
- In the non-combusting case, the mean velocity field past the dump plane is asymmetric with the formation of two unequal recirculation zones. The presence of combustion shortens the recirculation zones sizes and restores the symmetry in the case of the homogeneous reacting flow c_1. The mean flow field is asymmetric when an inlet equivalence ratio difference is introduced between the two incoming reactants streams.
- When the combustion is present in the combustor, the properties of the feeding channel flows are very dependent on the magnitude of the inlet equivalence ratio difference

between the two feeding streams. The presence of an equivalence ratio difference in the feeding flows, particularly for flow c_2, induces a noticeable increase of the total velocity fluctuations which is entirely due to the contribution of the coherent motion.

- In the combustor, in a general manner, the large-scale unsteadiness of the longitudinal velocity is progressively weakening with the development of the combustion. The spatial evolution of the fluctuation of the transverse velocity component proves also to be flow dependent, *i.e.*, the trend of its periodic motion energy distribution observed at the dump plane and in the near field is inverted in the far field, *i.e.*, further downstream, the coherent motion strength appears to be dominant at the side of the upper leaner reactants streams and in the central zone of the flow.
- Simultaneous two-point velocity measurements put into evidence that, in all cases, the two feeding streams are always pulsating longitudinally in phase.

A comprehensive database (available on DVD's) (including also detailed lean extinction properties and wall pressure measurements) has been constructed and is available upon request addressed to the corresponding author and can be sent after acceptance by the MOLECULES consortium. It gives access to both the processed and the raw (instantaneous) velocity data as well as to numerous "readme" files aimed at helping the database end-user, especially in the context of CFD benchmarking.

Acknowledgements

Part of this work has been supported by the European Project MOLECULES with Contract No. G4RD-CT-2000-00402 and the Région Poitou-Charentes (France). The experiments were carried out at Laboratoire de Combustion et de Détonique (UPR 9028 CNRS) in Poitiers (France) whose technical support is acknowledged. Nguyen, P.D. has been granted a postdoctoral fellowship by the Communauté d'Agglomération Pau-Pyrénées (France). The authors have benefited from helpful discussions with Dr. Duwig, C. (Lund University).

References

1. Correa, S.M.: Power generation and aero-propulsion gas turbines: from combustion science to combustion technology. *27th International Symposium on Combustion*, The Combustion Institute, Pittsburgh. 1793-1807 (1998).
2. Nguyen, P.D. and Bruel, P.: Turbulent reacting flow in a dump combustor: experimental determination of the influence of an inlet equivalence ratio difference on the contribution of the coherent and stochastic motions to the velocity field dynamics. *AIAA paper 2003-0958* (2003).
3. Nguyen, P.D.: Contribution expérimentale à l'étude des caractéristiques instationnaires des écoulements turbulents réactifs prémélangés stabilisés en aval d'un élargissement brusque symétrique. *Ph.D. thesis*, University of Poitiers, France (2003).
4. Roux, S., Lartigue, G., Poinsot, T., Meier, U. and Bérat, C.: Studies of mean and unsteady flow in a swirled combustor using experiments, acoustic analysis and large eddy simulations. *Combustion and Flame*. 141, 40-54 (2005).
5. Besson, M., Bruel, P., Champion, J.L. and Deshaies, B.: Experimental analysis of combusting flow developing over a plane symmetric expansion. *Journal of Thermophysics and Heat Transfer*. 14(1), 59-67 (2000).
6. Kurenkov, A. and Oberlack, M.: Modelling Turbulent Premixed Combustion Using the Level Set Approach for Reynolds Averaged Models. *Flow, Turbulence and Combustion*. 74, 387-407 (2005).
7. Bruel, P. and Nguyen, P.D.: Deliverable D3.12-1, Program MOLECULES, n° G4RD-CT-2000-00402. *Available upon request: Pascal.Bruel@univ-pau.fr*.
8. Domingo, P., Vervisch, L., Payet, S. and Hauguel, R.: DNS of a premixed turbulent V flame and LES of a ducted flame using a FSD-PDF subgrid scale closure with FPI-tabulated chemistry. *Combustion and Flame*. 143, 566-586 (2005).

9. Duwig, C., Salewski, M. and Fuchs, L.: Large eddy simulation of a turbulent flow past a pair of symmetric backward-facing steps: a sensitivity analysis. *AIAA paper 2007-0916* (2007).
10. Duwig, C. and Fureby, C.: Large eddy simulation of unsteady lean stratified premixed combustion. *Combustion and Flame*. 151, 85-103 (2007).
11. Duwig, C.: Study of a filtered flamelet formulation for large eddy simulation of premixed turbulent flames. Accepted for publication in *Flow, Turbulence and Combustion* (2007).
12. http://public.ca.sandia.gov/TNF/.
13. Lee, D.H. and Sung, H.J.: Assessment of turbulent bias in Laser Doppler velocimeter. *Experiments in Fluids*. 16(3-4), 223-225 (1994).
14. Benedict, L.H. and Gould, R.D.: Towards better uncertainty estimates for turbulence statistics. *Experiments in Fluids*. 22(2), 129-136 (1996).
15. Poinsot, T. and Veynante, D.: Theoretical and Numerical Combustion. Edwards, Philadelphia (2001).
16. Hussain, A.K.M.F. and Reynolds, W.C.: The mechanics of an organized wave in a turbulent shear flow. Part 1. *J. Fluid Mech.* 41(2), 241-258 (1970).
17. Hussain, A.K.M.F. and Reynolds, W.C.: The mechanics of an organized wave in a turbulent shear flow. Part 2: experimental results. *J. Fluid Mech*. 54(2), 241-261 (1972).
18. Korusoy, E. and Whitelaw, J.H.: Effects of wall temperature and gas on ducted premixed flames. *19th ICDERS*, Hakone, Japan. Paper 194, ISBN4-9901744-0-2 C3053 and ISBN4-9901744-1-0 C3053 (2003).
19. De Zilwa, S.R.N., Uhm, J.H. and Whitelaw, J.H.: Combustion oscillations close to the lean flammability limit. *Combustion Science and Technology*. 160, 231-258 (2000).

20. Abbott, D.E. and Kline, S.J.: Experimental investigation of subsonic turbulent flow over single and double backward facing steps. *Journal of Basic Engineering*. 84, 317-325 (1962).
21. Newland, D.E.: Random Vibrations, Spectral and Wavelet Analysis. Addison Wesley Longman Limited (1975).
22. Klein, M., Sadiki, A. and Janicka, J.: A digital filter based generation of inflow data for spatially developing direct numerical or large eddy simulations. *J. Comput. Phys*. 186, 652-665 (2003).
23. Biferale, L., Boffetta, G., Celani, A., Crisanti, A. and Vulpiani, A.: Mimicking a turbulent signal: sequential multiaffine processes. *Phys. Rev. E*. 57, 6261-6264 (1998).

List of Table Captions

List of Figure Captions:

Figure 1. Schematic of the entire ORACLES test rig and geometrical dimensions (in mm) at the entrance of the combustor.

Figure 2. Self-luminescence visualisations of the combustion zone just behind the dump plane with the first row for case c_1, the second row for case c_2 and the third row for case c_3; for each row: mean flame brush on the left with time exposure = 1/50s, remaining instantaneous flame brushes with time exposure = 1/500s.

Figure 3. Profiles of the mean streamwise and transverse velocities and of the related *rms*-velocity fluctuations normalised by the bulk velocity obtained in the feeding flows (maximum relative random error in $\overline{u}$ =±4%, $\overline{v}$ =±5%, $\overline{u'^2}$ =±12% and $\overline{v'^2}$ =±7%).

Figure 4. Profiles of the mean streamwise and transverse velocities and of related *rms*-velocity fluctuations normalised by the bulk velocity obtained at the dump plane (maximum relative random error in $\overline{u}$ =±3%, $\overline{v}$ =±5%, $\overline{u'^2}$ =±11% and $\overline{v'^2}$ =±8%).

Figure 5. Longitudinal evolution of the profiles of the mean streamwise and transverse velocities normalised by the bulk velocity obtained in the combustor (maximum relative random error in $\overline{u}$ =±3%, $\overline{v}$ =±6%).

Figure 6. Longitudinal evolution of the profiles of the *rms*-velocity fluctuations normalised by the bulk velocity obtained in the combustor (maximum relative random error in $\overline{u'^2}$ =±9% and $\overline{v'^2}$ =±7%).

Figure 7. Energy density spectra (EDS) of the streamwise velocity fluctuations at (x=-5h, y=1.51h) and (x=-5h, y=2.86h) for the flows considered (maximum resolution Δf=4.43Hz).

Figure 8. Probability density function (PDF) of the streamwise velocity at (x=-5h, y=1.51h) and (x=-5h, y=2.86h) for the flows considered (maximum resolution Δu=0.34m/s).

Figure 9. Profiles of the streamwise *rms*-velocity fluctuations (total u', stochastic u'_s and periodic u'_p) and of the relative contribution of the periodic coherent motion to the total streamwise velocity fluctuation energy Eu'_p, obtained at x=-5h for the flows considered.

Figure 10. Auto-correlation functions for streamwise fluctuating velocities (total u', periodic u'_p and stochastic u'_s) obtained at (x=-5.8h, y=1.51h) for the reactive flow c_1 (Λ_t is the integral time scale).

Figure 11. Energy density spectra (EDS) of the transverse velocity fluctuations at (x=0, y=1.51h), (x=0, y=2.18h) and (x=0, y=2.86h) for the reacting flows considered (maximum resolution Δf=6.31Hz).

Figure 12. Profiles of the streamwise and transverse *rms*-velocity fluctuations (total u', v', stochastic u'_s, v'_s and periodic u'_p, v'_p) and of the relative contribution of the periodic coherent motion to the total streamwise and transverse velocity fluctuation energy (Eu'_p, Ev'_p), obtained at the dump plane.

Figure 13. Cartographies of the relative contribution of the coherent periodic motion at the dominant fundamental frequency of around 50Hz to the local total energy of the streamwise (Eu'_p) and transverse (Ev'_p) velocity fluctuations.

Figure 14. Crosswise profiles of the two-point correlation coefficient $Ru'_A u'_y$ for the streamwise velocity fluctuations (total, stochastic and periodic), obtained at x=-5h for the lower inlet channel and at the dump plane x=0.

TABLES:

Table 1. Main parameters of the test cases (atmospheric pressure, temperature of the incoming flows = 276±11K; systematic error in mass flow rate Q=±1g/s and in equivalence ratio Φ=±0.02, relative uncertainty in Re=±2% and in U_{bulk}=±1.5%) and characteristic numbers and length scales.

Flow	**Stream**	**Re**	**Q** g/s	**U_{bulk}** m/s	**Φ**	**Thermal Power** kW	**Da**	**Ka**	**λ_x** $.10^3$ m	**η_K** $.10^6$ m
nc1	Upper	25000	65	11	-	-	-	-	2.2	111
	Lower	25000	65	11	-	-	-	-	1.8	103
c1	Upper	25000	65	11	0.75	110	11.1	3.4	2.5	103
	Lower	25000	65	11	0.75	110	10.6	3.0	2.4	110
c2	Upper	25000	65	11	0.70	105	6.0	8.1	2.4	88
	Lower	25000	65	11	0.80	116	15.2	2.9	2.4	94
c3	Upper	25000	65	11	0.65	98	3.0	11.2	2.4	115
	Lower	25000	65	11	0.85	121	17.7	1.5	2.3	114

Table 2. Flow parameters defining the four differents configurations investigated to search the lean extinction limit (atmospheric pressure, temperature of the incoming flows = 276±11K; systematic error in mass flow rate Q=±1g/s and in equivalence ratio Φ_L^{ext} or Φ_U^{ext} =±0.02).

	Re_U (/ 10^3)	**Re_L (/ 10^3)**	**ΔRe (/ 10^3)**	**Q_U (g/s)**	**Q_L (g/s)**	Φ_U^{st}	Φ_L^{st}	Φ_U^{ext}	Φ_L^{ext}
Situation 1	25-65	25-65	0	65-169	65-169	0.65	0.60	0.54-0.56	-
	25-75	25-75	0	65-195	65-195	0.65	0.65	0.51-0.57	-
	25-65	25-65	0	65-169	65-169	0.65	0.70	0.54-0.56	-
	25-65	25-65	0	65-169	65-169	0.65	0.75	0.54-0.56	-
Situation 2	25-75	25-75	0	65-195	65-195	0.65	0	0.53-0.57	-
Situation 3	25-75	25-75	0	65-195	65-195	0.65	0.65	0.54-0.57	0.54-0.57
Situation 4	25-50	30-75	5-45	65-130	78-195	0.65	0.65	0.52-0.56	-

Table 3. Mean reattachment length of the recirculation zones for the different flows considered.

Case	Length of lower recirculation zone (estimated from interpolation)	Length of upper recirculation zone (estimated from interpolation)
nc_1	5.5h	8.0h
c_1	2.3h	2.3h
c_2	2.3h	2.5h
c_3	1.9h	2.8h

FIGURES:

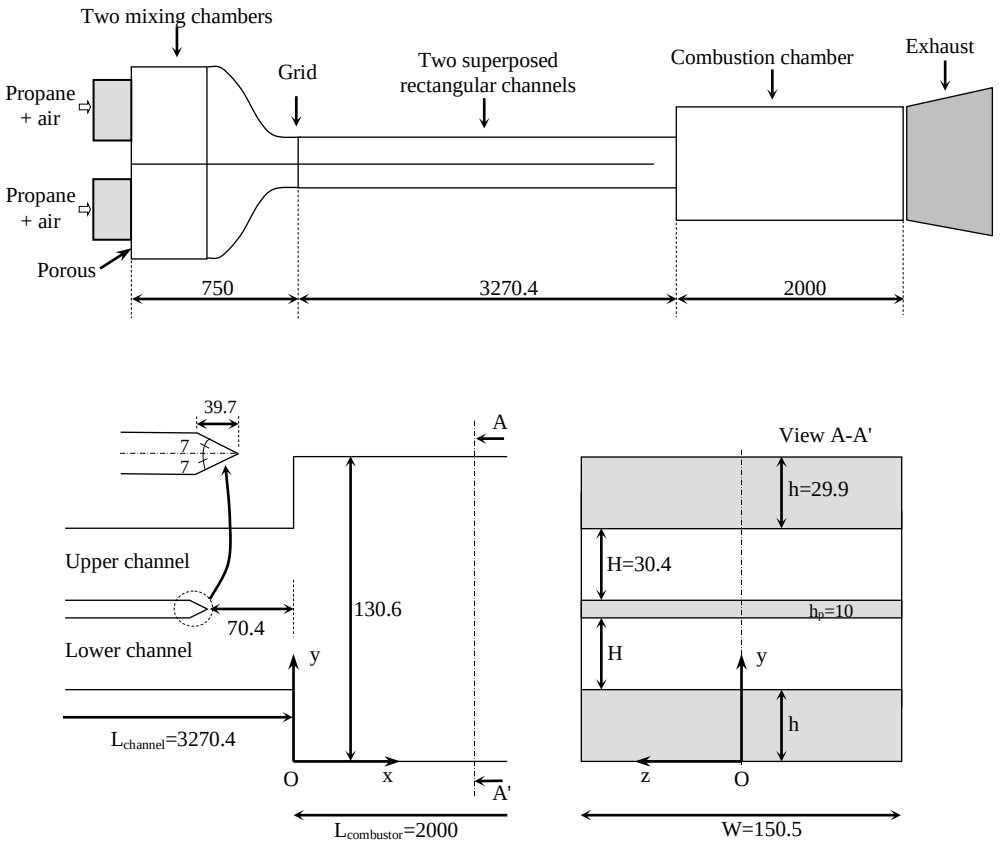

Figure 1. Schematic of the entire ORACLES test rig and geometrical dimensions (in mm) at the entrance of the combustor.

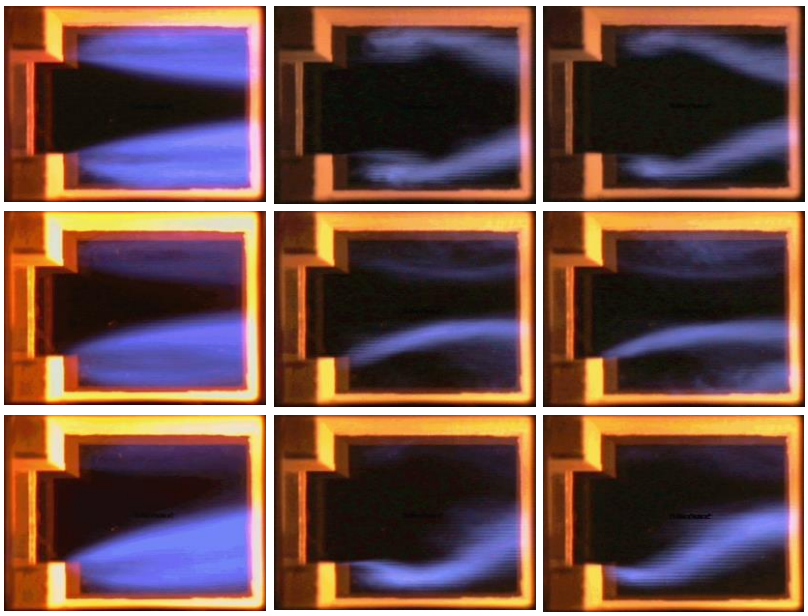

Figure 2. Self-luminescence visualisations of the combustion zone just behind the dump plane with the first row for case c_1, the second row for case c_2 and the third row for case c_3; for each row: mean flame brush on the left with time exposure = 1/50s, remaining instantaneous flame brushes with time exposure = 1/500s.

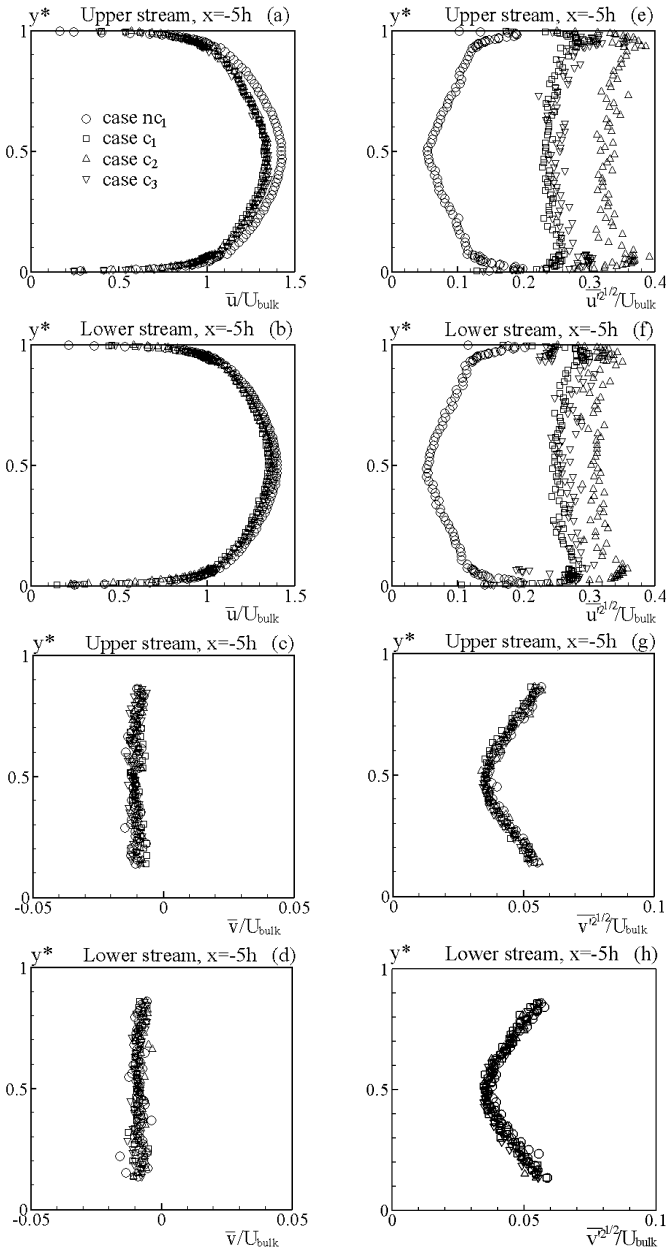

Figure 3. Profiles of the mean streamwise and transverse velocities and of the related *rms*-velocity fluctuations normalised by the bulk velocity obtained in the feeding flows (maximum relative random error in $\bar{u}$ =±4%, $\bar{v}$ =±5%, $\overline{u'^2}$ =±12% and $\overline{v'^2}$ =±7%).

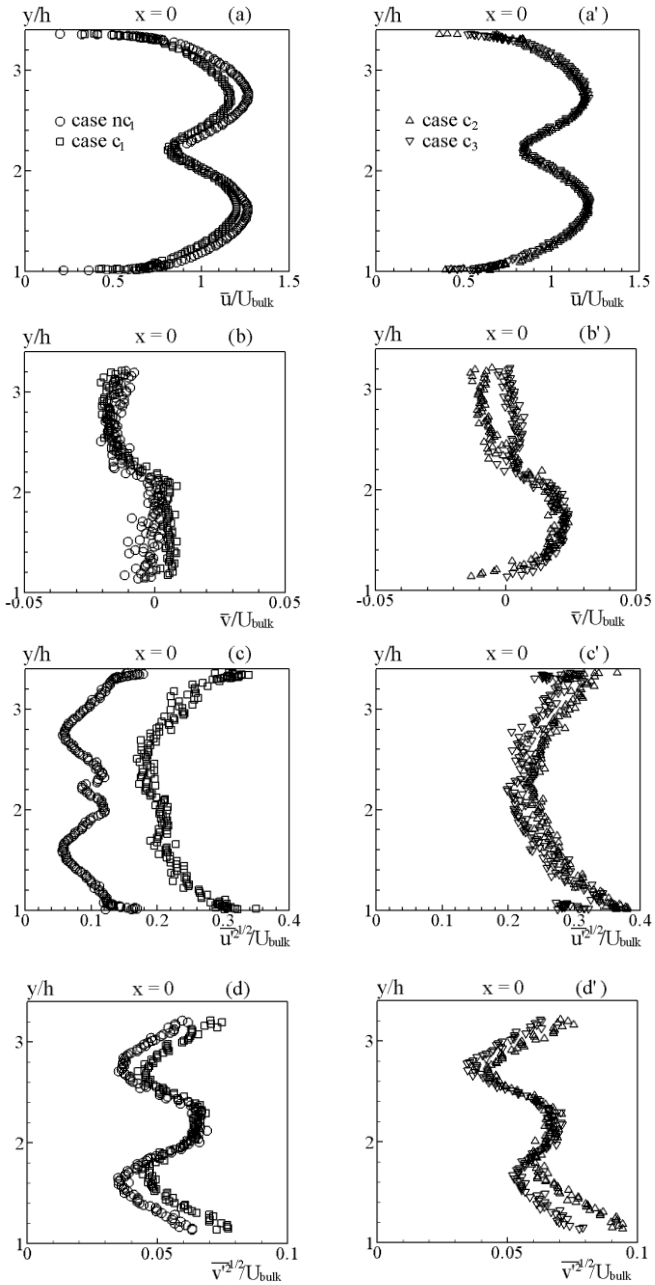

Figure 4. Profiles of the mean streamwise and transverse velocities and of related *rms*-velocity fluctuations normalised by the bulk velocity obtained at the dump plane (maximum relative random error in $\overline{u}$ =±3%, $\overline{v}$ =±5%, $\overline{u'^2}$ =±11% and $\overline{v'^2}$ =±8%).

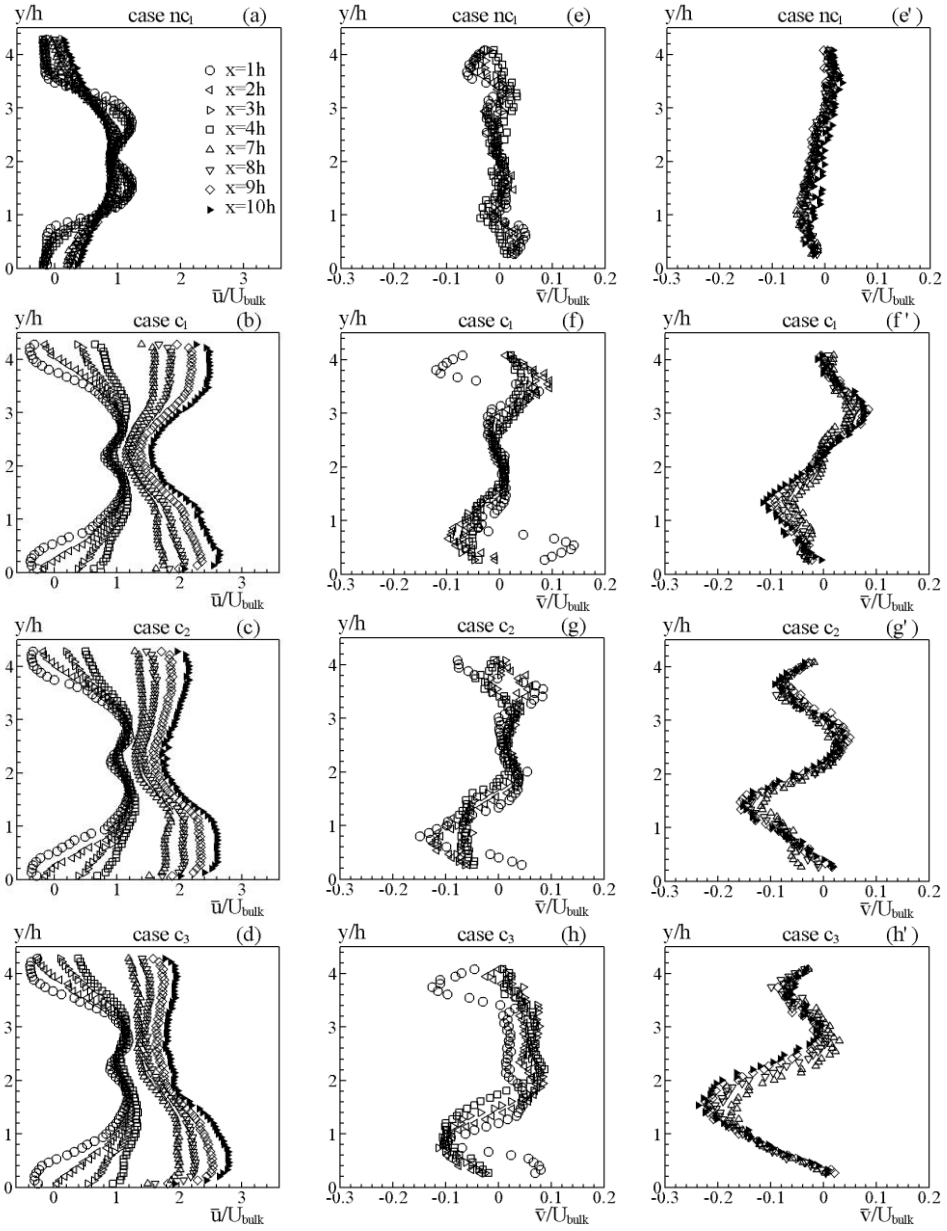

Figure 5. Longitudinal evolution of the profiles of the mean streamwise and transverse velocities normalised by the bulk velocity obtained in the combustor (maximum relative random error in $\overline{u}$ =±3%, $\overline{v}$ =±6%).

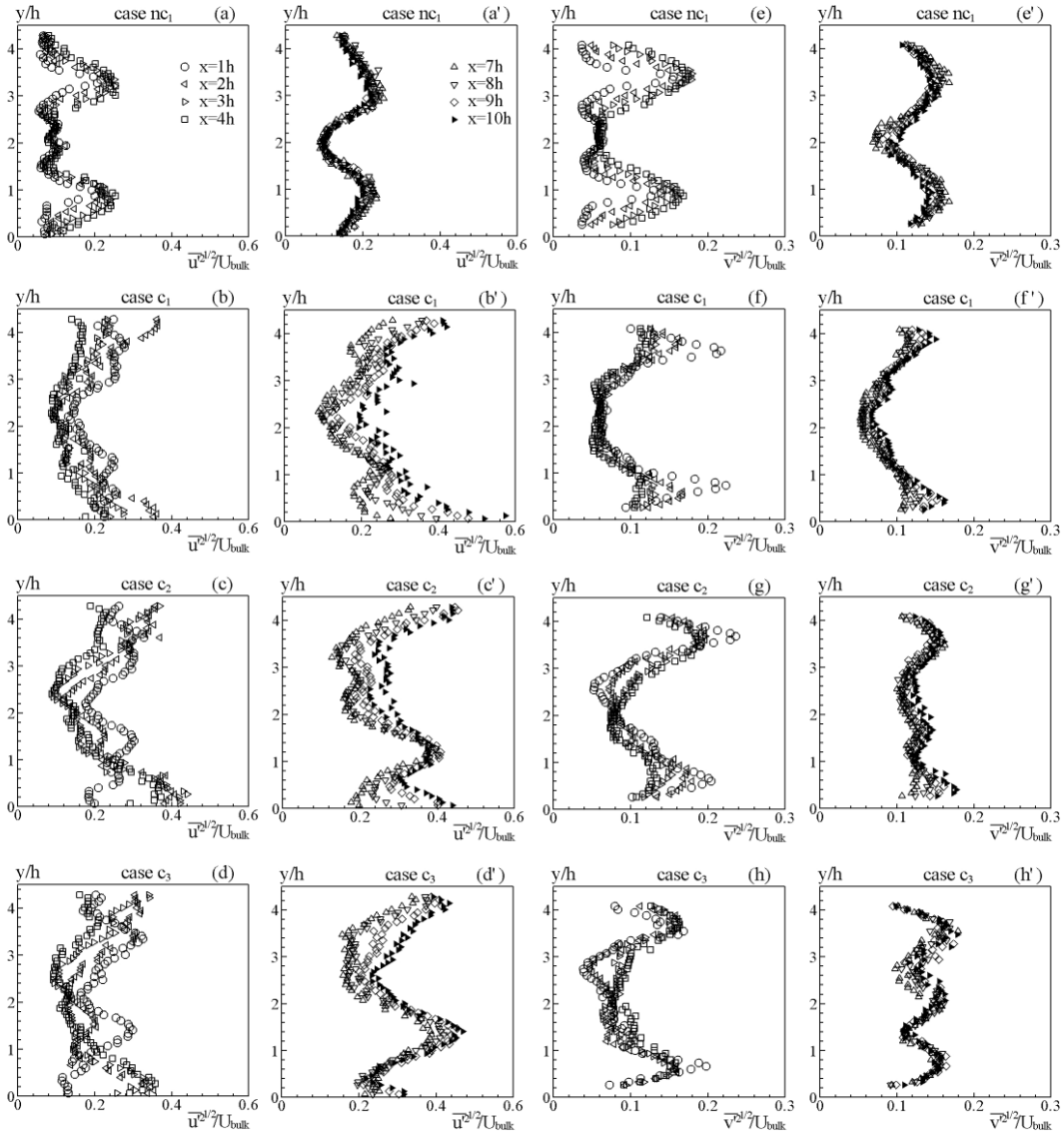

Figure 6. Longitudinal evolution of the profiles of the *rms*-velocity fluctuations normalised by the bulk velocity obtained in the combustor (maximum relative random error in $\overline{u'^2}$ =±9% and $\overline{v'^2}$ =±7%).

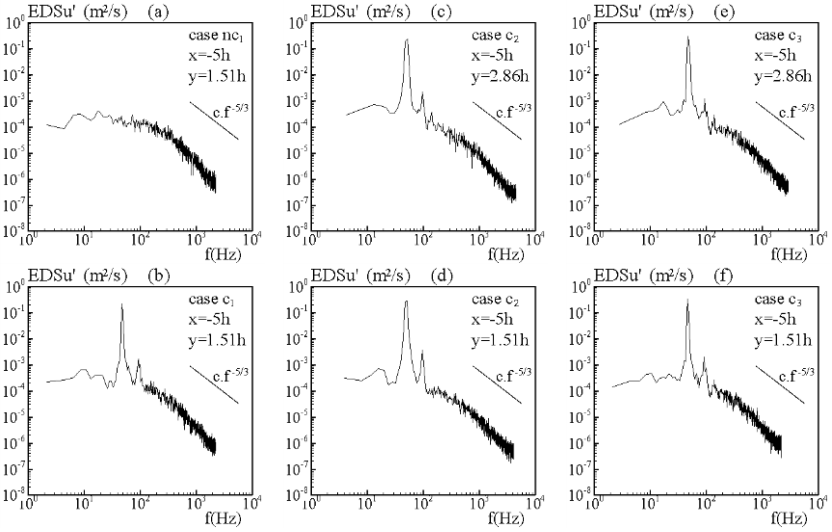

Figure 7. Energy density spectra (EDS) of the streamwise velocity fluctuations at (x=-5h, y=1.51h) and (x=-5h, y=2.86h) for the flows considered (maximum resolution Δf=4.43Hz).

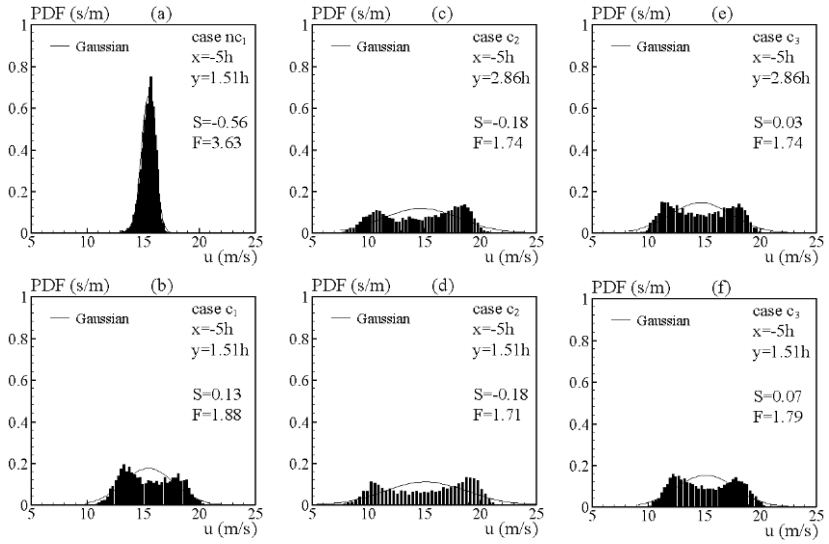

Figure 8. Probability density function (PDF) of the streamwise velocity at (x=-5h, y=1.51h) and (x=-5h, y=2.86h) for the flows considered (maximum resolution Δu=0.34m/s).

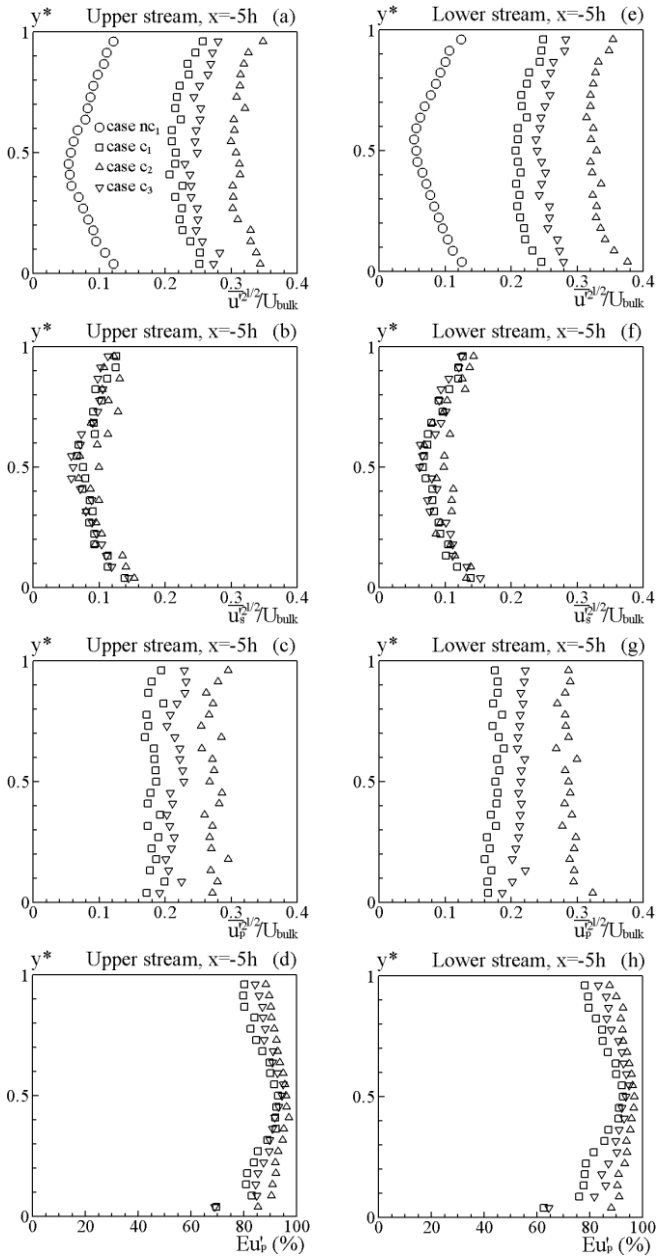

Figure 9. Profiles of the streamwise *rms*-velocity fluctuations (total u', stochastic u'_s and periodic u'_p) and of the relative contribution of the periodic coherent motion to the total streamwise velocity fluctuation energy Eu'_p, obtained at x=-5h for the flows considered.

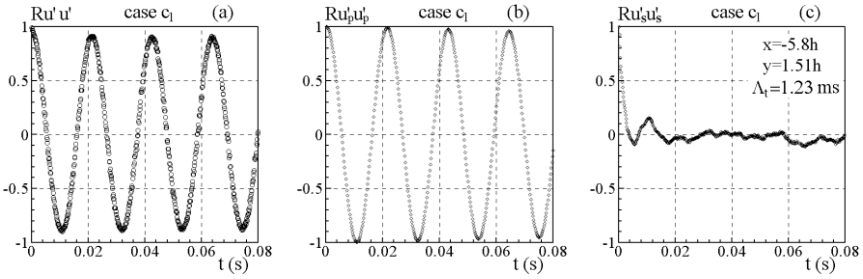

Figure 10. Auto-correlation functions for streamwise fluctuating velocities (total u', periodic u'_p and stochastic u'_s) obtained at (x=-5.8h, y=1.51h) for the reactive flow c_1 (Λ_t is the integral time scale).

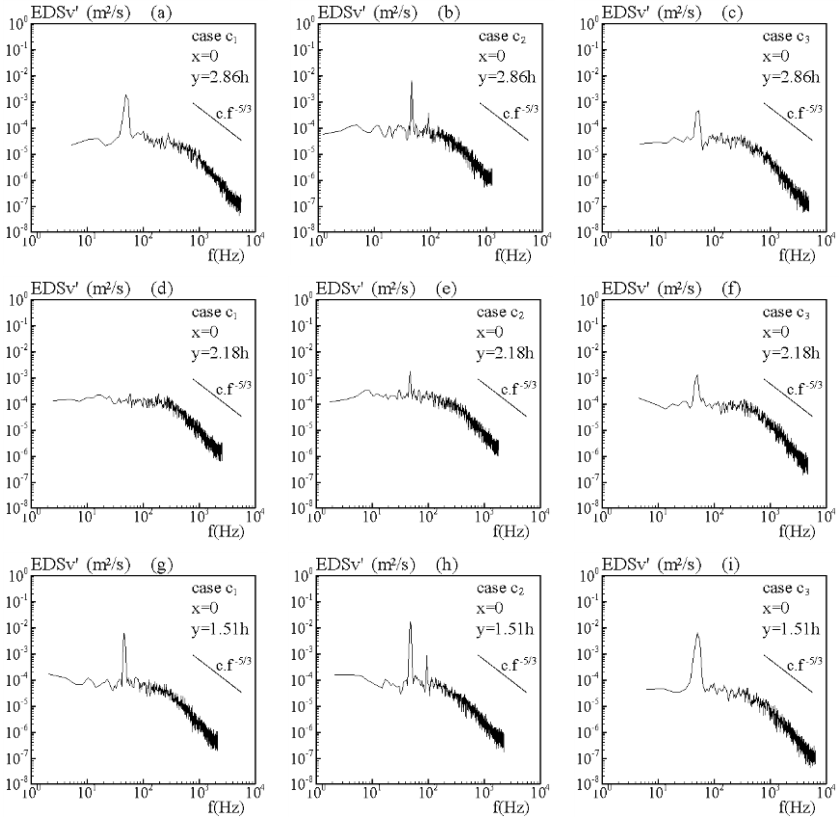

Figure 11. Energy density spectra (EDS) of the transverse velocity fluctuations at (x=0, y=1.51h), (x=0, y=2.18h) and (x=0, y=2.86h) for the reacting flows considered (maximum resolution Δf=6.31Hz).

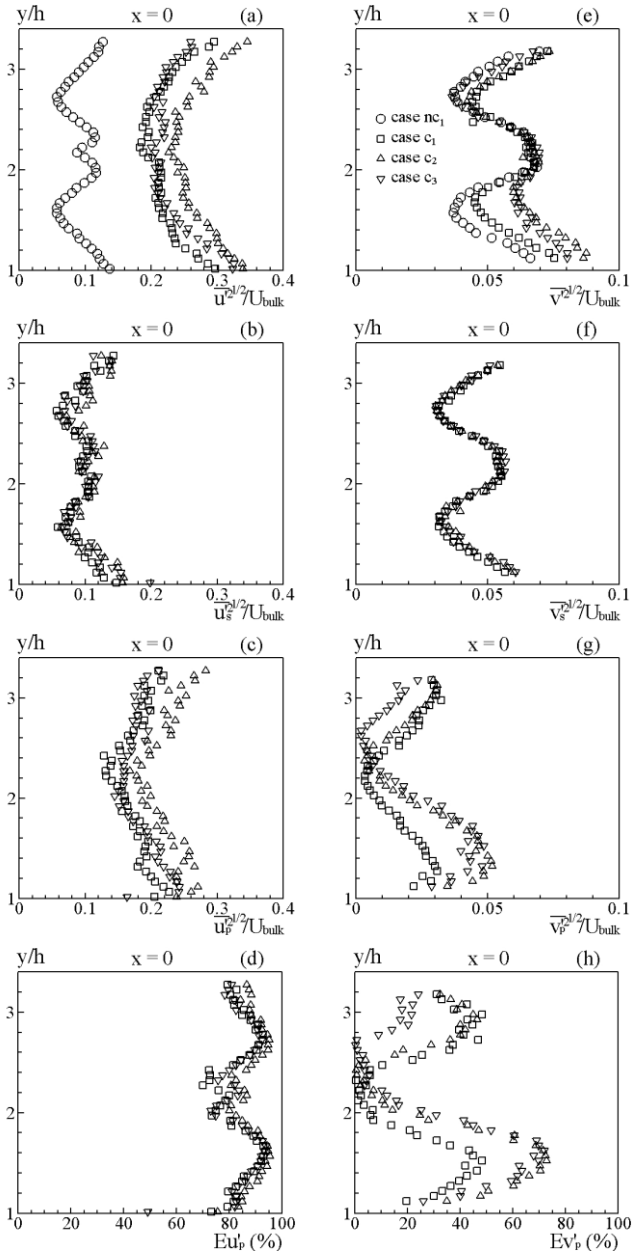

Figure 12. Profiles of the streamwise and transverse *rms*-velocity fluctuations (total u', v', stochastic u'_s, v'_s and periodic u'_p, v'_p) and of the relative contribution of the periodic coherent motion to the total streamwise and transverse velocity fluctuation energy (Eu'_p, Ev'_p), obtained at the dump plane.

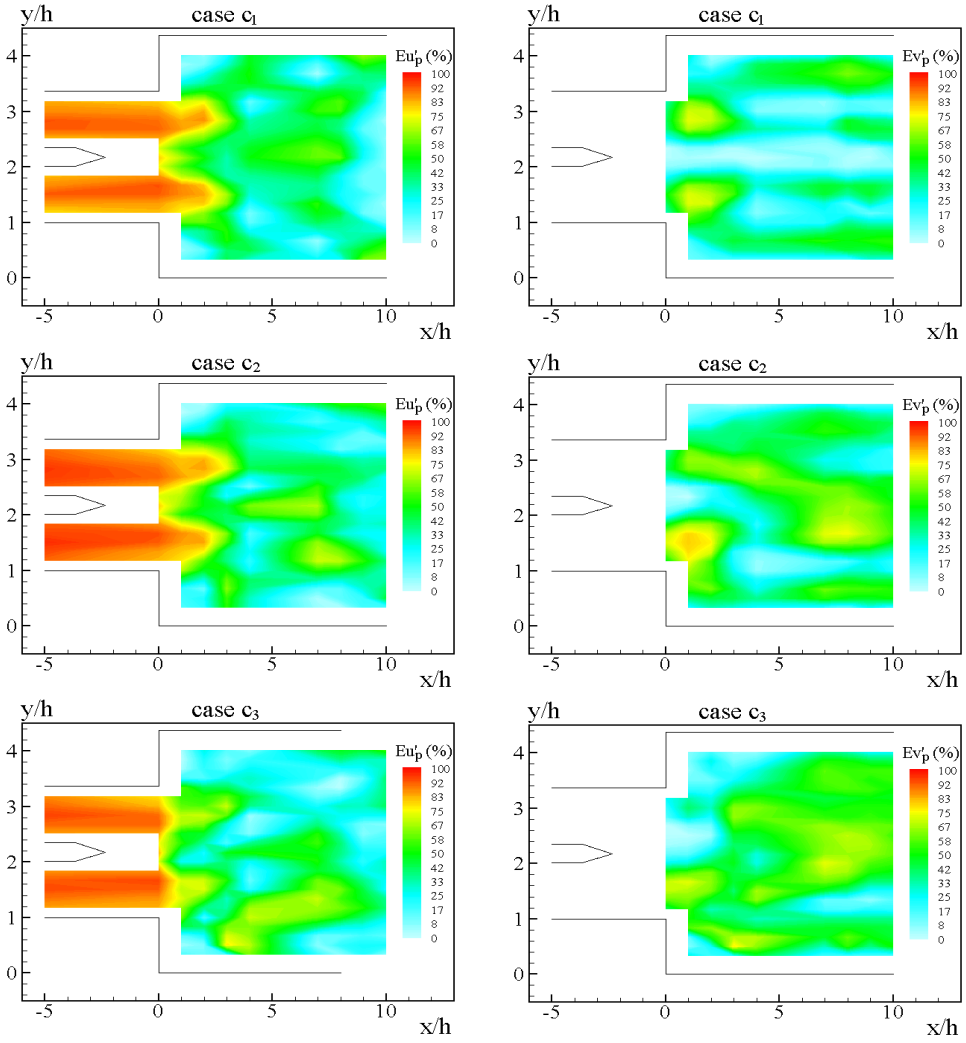

Figure 13. Cartographies of the relative contribution of the coherent periodic motion at the dominant fundamental frequency of around 50Hz to the local total energy of the streamwise (Eu'_p) and transverse (Ev'_p) velocity fluctuations.

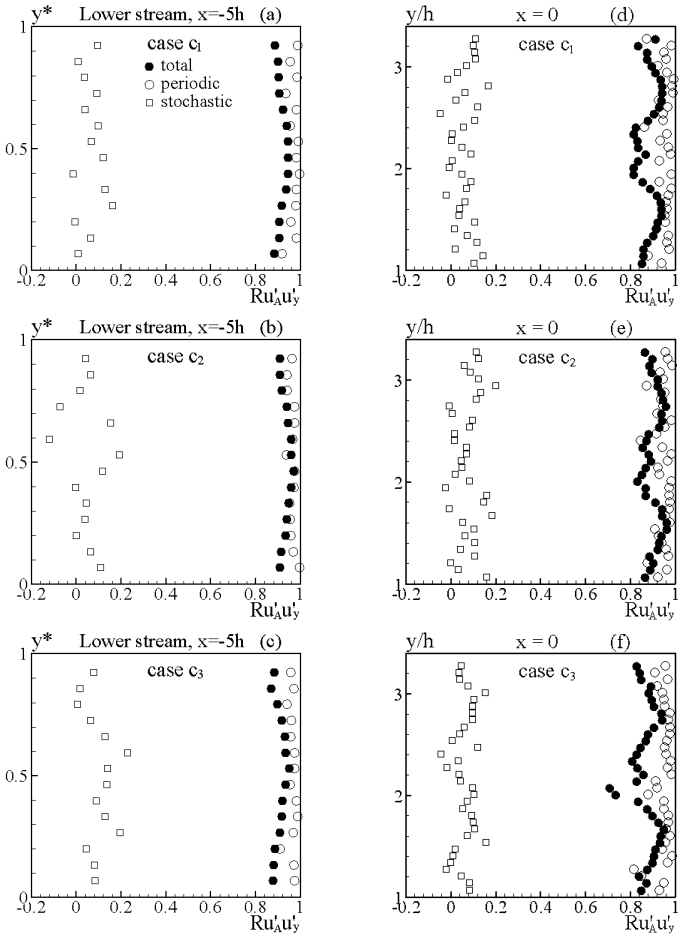

Figure 14. Crosswise profiles of the two-point correlation coefficient $Ru'_A u'_y$ for the streamwise velocity fluctuations (total, stochastic and periodic), obtained at x=-5h for the lower inlet channel and at the dump plane x=0.